JJEE

Volume 10 | Number 2 | June 2024 | Pages 212-228

Jordan Journal of Electrical Engineering

ISSN (print): 2409-9600, ISSN (online): 2409-9619

Homepage: jjee.ttu.edu.jo

A Spiral Flower Shape Wearable Antenna for Smart Internet of Things Applications

Ala'a Al-laymoun[1], Rula Alrawashdeh[2*]

[1, 2] Electrical Engineering Department, College of Engineering, Mutah University, Alkarak, Jordan

E-mail: rularsr18@gmail.com

Received: Jun 01, 2023 *Revised: Sep 02, 2023* *Accepted: Sep 12, 2023*

***Abstract*—** In this paper a small patch antenna is proposed for smart wearable internet of things (IoT) applications. The antenna is proposed to be the main piece of a necklace. It works for the 2.4 - 2.5 GHz industrial, scientific and medical (ISM) band. It also works for other bands such as 5.564 - 5.65 GHz, 6.79 - 6.973 GHz, 7.7614 - 7.883 GHz and 8.5 - 8.65 GHz with a small size of 40 × 50 mm² and robust performance. The proposed design showed to have many appealing features such as small size, conformity and multi-band functionality and, thus, it could be a good candidate for IoT wearables.

***Keywords*—** Internet of things; Specific absorption rate; Spiral flower; Wearable antennas.

1. INTRODUCTION

Internet of Things (IoT) enabled medical wearables to provide individuals with the information needed to achieve better health outcomes such as real-time health monitoring. An example of an IoT based healthcare system is shown in Fig. 1. In such a system, data collected from different wearable sensors such as blood pressure and heart rate monitoring sensors are sent over the IoT cloud to the doctor who takes actions regarding the patient's health accordingly. Also, such a system enables data storage on a centralized cloud/server to be later analyzed for better healthcare services. Real time alerts are sent back to the patient based on the analyzed data. Such a system helps in improving the level of healthcare services by providing real-time monitoring, quick treatment, and cost reduction of using the hospital's resources and hospital visits [1].

Data are usually sent from the wearable sensor using an antenna to the cloud over the mobile network. The wearable antenna is required to be: compact in size, light in weight, conformal, safe, reliable in connectivity, and easy to integrate within the IoT device [2]. The antenna should also satisfy the Specific Absorption Rate limitations (1g SAR < 1.6 W/kg or 10g SAR< 2 W/kg) [3]. Different wearable antennas of different types were proposed for IoT applications such as smart watches [4], smart glasses [5], bracelets [6], finger rings [7], and Bluetooth headsets [8]. These antennas were mainly proposed for the 2.45 GHz Industrial Scientific Band (ISM) band. Although the proposed designs have exploited the structure effectively, detuning was observed in most of the proposed designs [8]. Wearable necklace antennas were also proposed in [9-10]. The antenna in [9] was designed to work at 29 GHz at which free space losses are high. Moreover, it was not evaluated as a wearable piece on a human body model. The wearable necklace antennas in [10] had no ground and thus their radiation

* Corresponding author

DOI: https://doi.org/10.5455/jjee.204-1685620635

was reduced considerably after testing them on the human body. Generally, as there is an increased interest in smart home applications based on IoT, more designs are needed to enable a wider spread of the application. Thus, a new conformal design for IoT applications is proposed in this paper. The antenna is designed to be the main piece of a necklace with overall dimensions of 40×50 mm². The proposed antenna has shown a robust performance on a skin layer. The design went through four steps of optimization which can inspire other designs for similar applications.

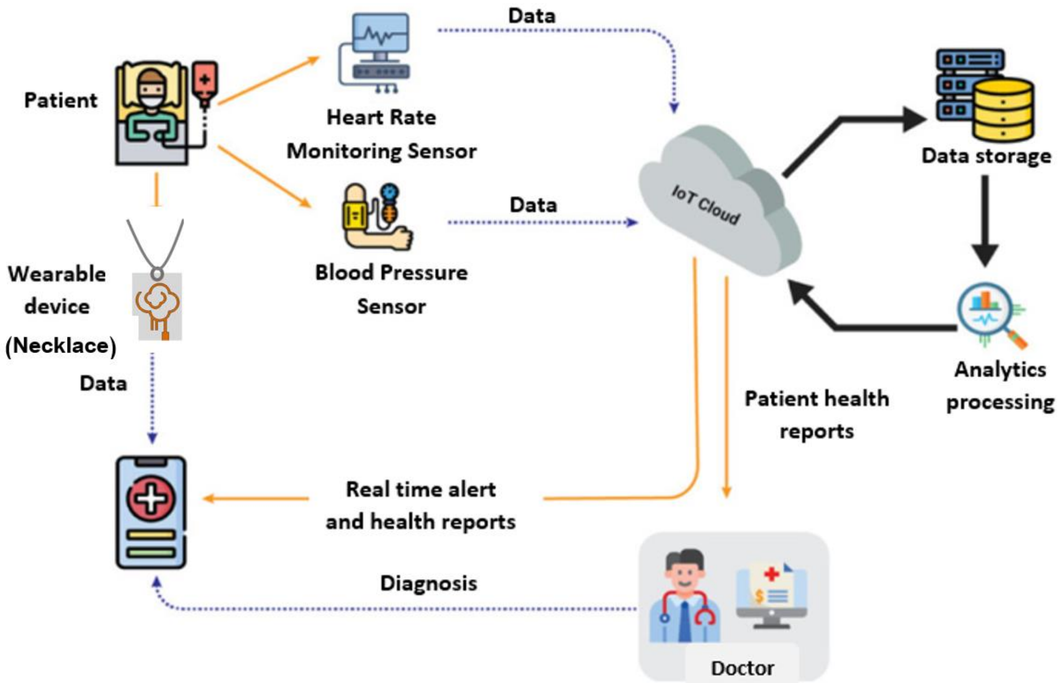

Fig. 1. IoT based healthcare system [1].

The paper is arranged as follows: First, the design requirements and techniques are described. Then, the performance is analyzed and discussed. The paper is concluded at the end.

2. THE ANTENNA DESIGN

In this section, the antenna parameters and design steps are presented as follows:

2.1. Design Requirements

The antenna is required to be:

a) Conformal to the wearable device. It should utilize the available structure effectively without adding extra weight or complexity to the design. Hence, the proposed antenna is designed to be a part of a wearable necklace. The necklace has been selected because it is light in weight, and it can be easily integrated into people's daily life. The patch over which this antenna is built will be the main piece of embellishment attached to the necklace. It has a rectangular shape.

b) Small in size. The antenna is aimed for a maximum size of 50×40 mm². This is to fit in the necklace without making it big.

c) Well matched (S_{11}< -10 dB) over the entire band of 2.4-2.5 GHz which is usually exploited for such applications [11]. This is obtained following different steps as will be explained in the following sections.

d) Of a robust performance when placed over the skin. The antenna should maintain good matching and radiation characteristics on the skin. The ground in the design will contribute to reduce the power absorption caused by the human body's skin.

2.2. Design Technique and Steps

8The antenna proposed in this paper is designed using the Computer Simulation Technology (CST) software package [12]. Hexahedral meshes and time domain solver are employed. The antenna is fed by a waveguide port of 50 Ω with an input power of 1 W. The design steps to satisfy the design requirements mentioned above can be summarized as follows: Step 1: Make an initial design based on the intended dimensions and structure. A spiral of flower like shape is created on a small patch of 50 mm × 40 mm dimensions and on a dielectric substrate of a relative permittivity of 4.3 and thickness of 1.6 mm. The initial structure is shown in Fig. 2. A spiral shape is selected because it tends to increase the near magnetic field which is reflected on increasing the antenna gain and improving its radiation capabilities [13].

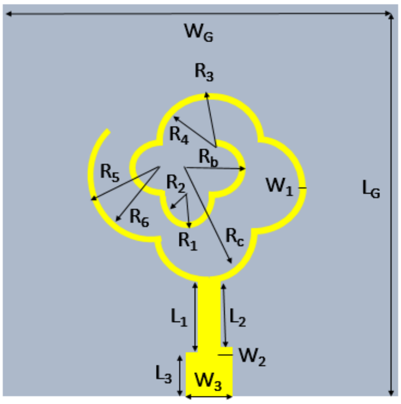

Fig. 2. Initial antenna structure (R_1= 3, R_2= 2, R_3= 5, R_4= 4, R_5= 6, R_6 = 5, R_b= 5, R_c= 12, L_G= 40, W_G= 50, L_1= 5.12, L_2= 5, L_3 = 4, W_1= 1, W_2= 0.9, W_3=3.065 (dimensions in mm).

Two locations of the feedline are attempted: one centered at the spiral half, and another one at 2 mm to the right of the first location. The simulated reflection coefficient is shown in Fig. 3.

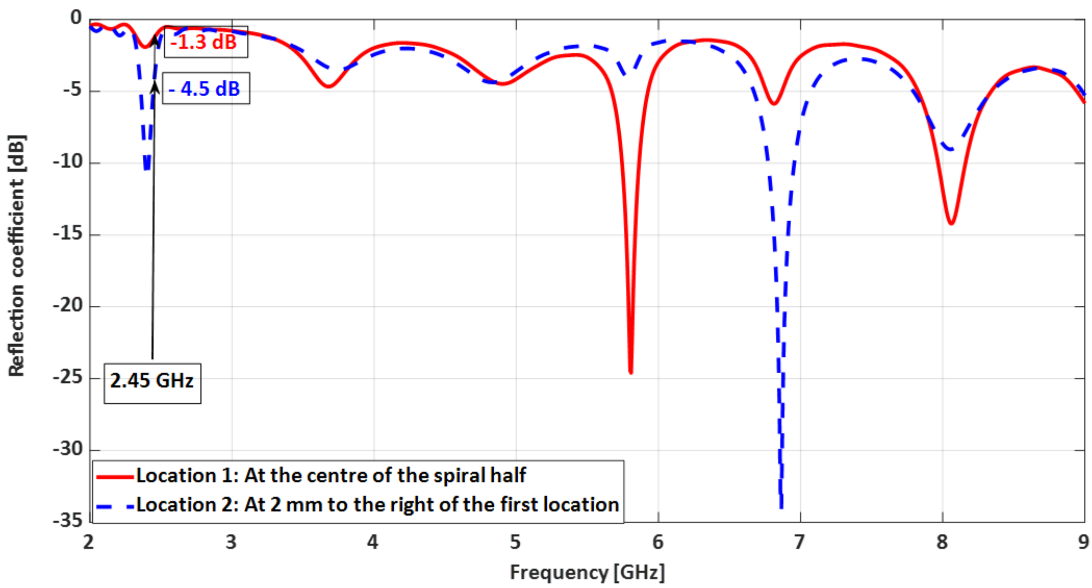

Fig. 3. The reflection coefficient S_{11} at two locations for the antenna in step 1.

The results in the figure indicate that matching is still not very ideal at 2.45 GHz at this stage. The reflection coefficient results are -1.3 and -4.5 dB at 2.45 GHz for the locations at the center of the spiral half, and at 2 mm to the right of the first location, respectively which are still larger than -10 dB. The reflection coefficient is required to be smaller than -10 dB (S_{11} < -10 dB) to ensure that 10% or less of the input power provided to the antenna is only reflected [14].

$$S_{11}(dB) = 10log_{10}\left(\frac{P_{ref}}{P_{in}}\right) \quad (1)$$

where P_{ref} (W) is the reflected power and P_{in} (W) is the input power provided to the antenna.

The feedline location is found to affect the matching. The matching was improved when the line was shifted to the right. The design is modified based on that in the next stage.

The resonance is mainly influenced by the following parameters:

1) Overall length of the spiral (L (m)):

$$f_r = \frac{c}{L} \quad (2)$$

where c (m/s) if the speed of electromagnetic waves in free space and f_r (Hz) is the resonant frequency.

This length has been calculated as 188.5 mm as follows:

$$L = 3 \times (2\pi R_1) + 3 \times (2\pi R_3) + (2\pi R_5) \quad (3)$$

where R_1, R_3 and R_5 are the radii introduced with their values in Fig. 2.

The overall length was set mainly to obtain resonance at around 2.45 GHz. When this length is increased the resonant frequency will shift down and the opposite occurs when this length is decreased.

2) Spacing between the spiral rings which is mainly controlled by R_b and R_c which are introduced on the structure in Fig. 2. The inner and outer ring layers can resemble the plates of a circular capacitor of which the capacitance (C_c(F)) is controlled as in Eq. (4) [15]:

$$C_c = \frac{4\pi\varepsilon}{\frac{1}{R_b} - \frac{1}{R_c}} \quad (4)$$

where ε (F/m) is the permittivity.

It is obvious from the equation that the values of R_b and R_c affect the capacitance and their values are set to obtain resonance at the intended frequencies.

The capacitance (C_c) controls the resonant frequency f_r(Hz) as in Eq. (5) [16]:

$$f_r = \frac{1}{2\pi\sqrt{LC_c}} \quad (5)$$

where L (H) is the overall inductance of the structure.

Step 2: Improve the antenna matching to obtain S_{11}< -10 dB at 2.45 GHz. This is obtained by: 1) adjusting the location of the feed line in correspondence with the work in [17-18] and based on the results of the previous step. The new location is centered at about 4.6 mm to the right with dimensions between (3.063–6.13) mm, and 2) cropping a small section (0.7×1) mm from the inner spiral ring. Cropping the indicated part works to control the antenna capacitance and thus to improve the antenna matching. The edges of the inner spiral ring can resemble the plates of a parallel plate capacitor. When some part of it is cropped, the distance between the plates (d (m)) increases which reduces the capacitance (C_P (F)) for this case [15].

$$C_P = \frac{\varepsilon A}{d} \quad (6)$$

where A (m^2) is the plate area which is not affected by cropping the above-mentioned part.

The final location of the feed line and the dimension of the cropped section are selected based on a parametric sweep conducted via CST. The antenna structure at this stage is shown in Fig. 4. The reflection coefficient is shown in Fig. 5. The antenna obtained a reflection coefficient of -19.2 dB at 2.45 GHz which is below the -10 dB targeted value.

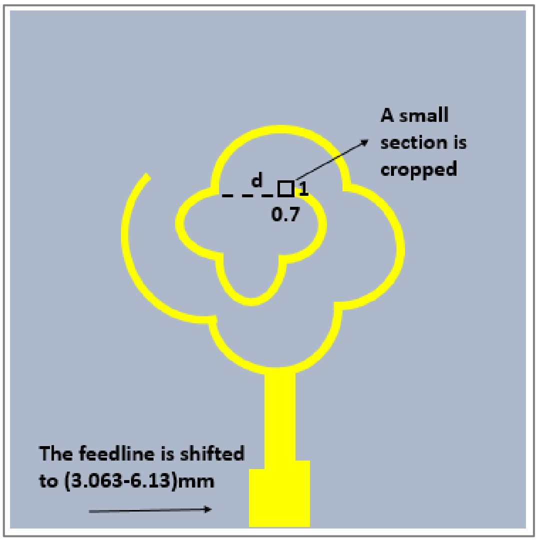

Fig. 4. The antenna structure in step 2 (dimensions in mm).

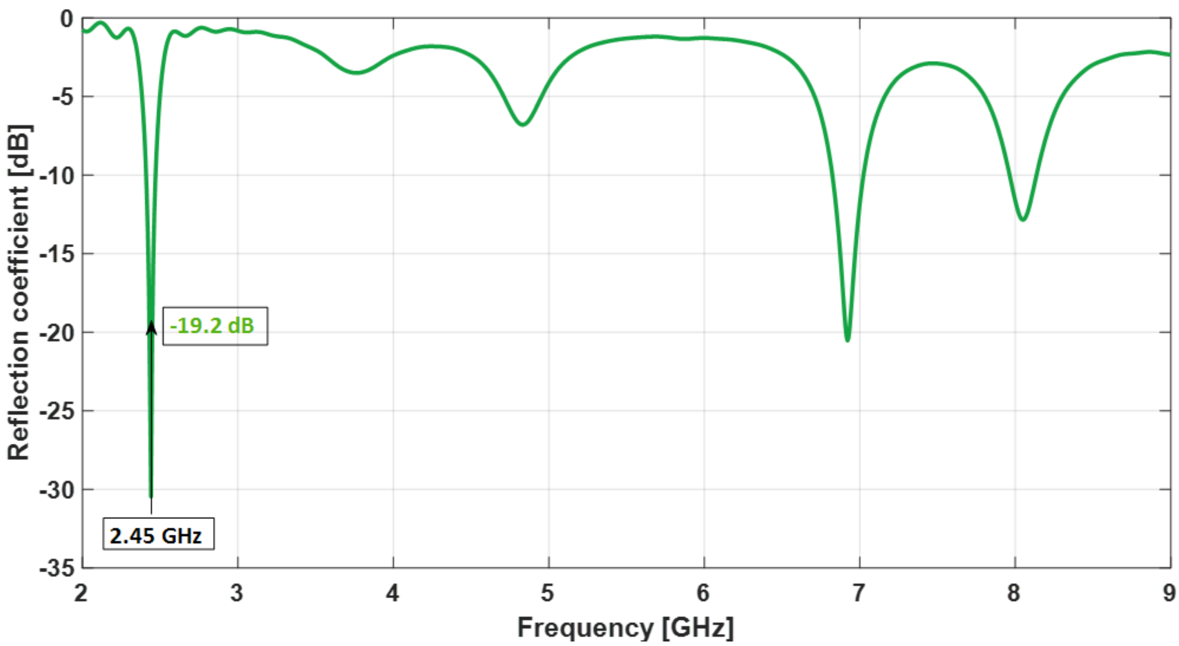

Fig. 5. The reflection coefficient S_{11} for the antenna in step 2.

Step 3: Obtaining other frequency bands. To obtain this, two lines are added to the left bottom side of the outer spiral ring as shown in Fig. 6 in correspondence with the work in [19-20]. The two locations of the lines are carefully chosen based on a parametric sweep to obtain the targeted matching. The two lines are added one by one. When the first line is added, a bit deeper matching (S_{11}= -20.8 dB) is obtained at 2.45 GHz. Other frequency bands ((4.4748-4.577), (6.79-6.973) and (8.384-8.62) GHz) are also obtained as shown in Fig. 6. The added line generates a new resonant frequency. When the second line is added to the proposed design, the antenna matching is improved (S_{11}< -10 dB) at the (5.569-5.669) GHz band. This is due to the capacitive coupling between the second line with the initial one. This band is already of interest for wireless communication, particularly the IoT applications [21].

A new resonant frequency is also introduced at (7.7614-7.883) GHz as shown in Fig. 7.

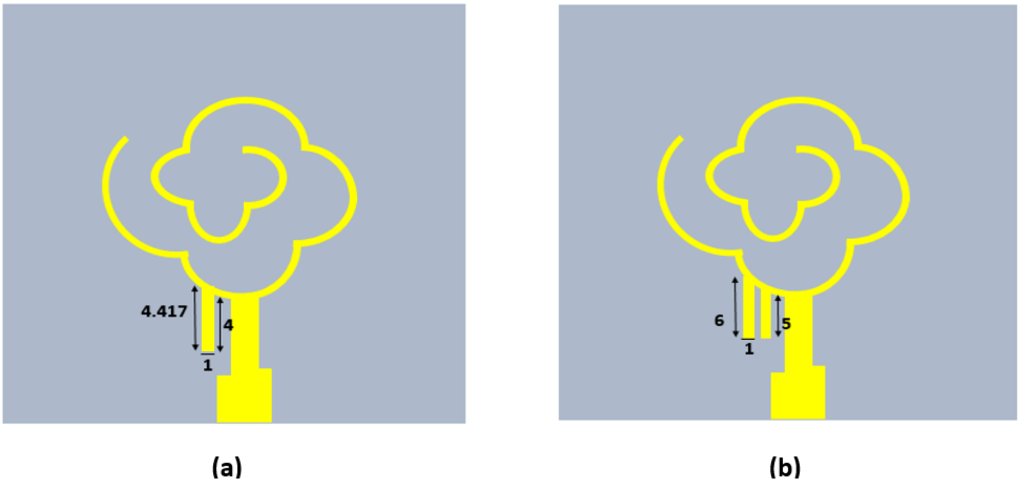

Fig. 6. The modified antenna structure with the added lines (dimensions in mm): a) first strip only; b) two strips.

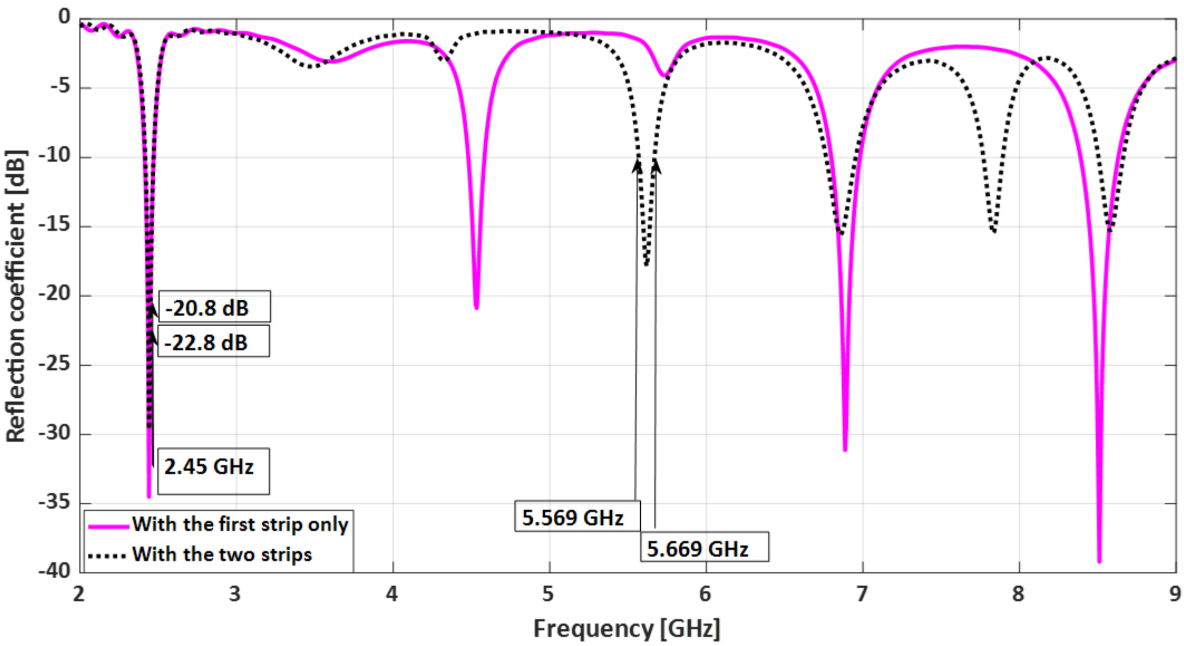

Fig. 7. The reflection coefficient S_{11} of the antenna with the first strip only, and with two strips.

The final antenna structure is shown in Fig. 8 and its parameters are summarized in Table 1. It is worth indicating that the final dimensions of the feedline are computed using CST to obtain a line impedance of 50 Ω. The transition made in the transmission line is intended to obtain deeper matching at the higher frequency bands ((6.79-6.973), (7.7614-7.883) and (8.5-8.65)) GHz.

Step 4: Simulation on a model of a skin layer. The antenna is simulated on a skin layer shown in Fig. 9. The skin layer has a rectangular shape of (90×90×3 mm^3) in size. It has a relative permittivity of 38 and conductivity of 1.464 (S/m) which resembles the dielectric properties at 2.45 GHz [22]. The antenna is placed at the center on the top skin layer. The reflection coefficient S_{11} (dB) for this case is shown in Fig. 10. It can be seen from the figure that the antenna works very well with a good matching for all the intended frequency bands that were achieved in free space. This is attributed to the antenna ground that preserves the antenna performance and reduces the human body effect.

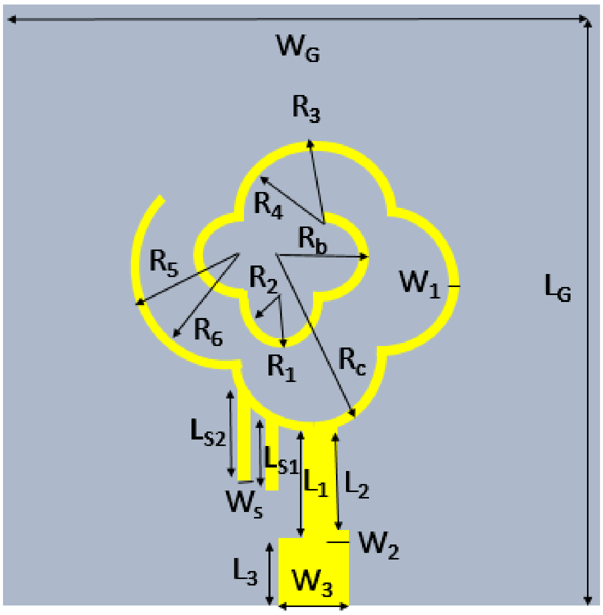

Fig. 8. The final antenna structure.

Table 1. Parameters of the final optimized antenna.

Parameter	Symbol	Value [mm]
Ground width	W_G	50
Ground length	L_G	40
The outer radius of inner rings	R_1	3
The inner radius of inner rings	R_2	2
The outer radius of outer rings	R_3	5
The inner radius of outer rings	R_4	4
The outer radius of the edge ring	R_5	6
The inner radius of the edge ring	R_6	5
Radius from center to the outer boundary of the inner rings	R_b	5
Radius from center to the outer boundary of the outer rings	R_c	12
Length of the upper feedline left edge	L_1	5.12
Length of the upper feedline right edge	L_2	5
Length of the lower feedline left edge	L_3	4
Width of the top right edge of the lower feedline	W_2	0.9
Width of the lower feedline bottom	W_3	3.065
Length of the left added line	L_{s2}	6
Length of the right added line	L_{s1}	5
Width of each added line	Ws	1

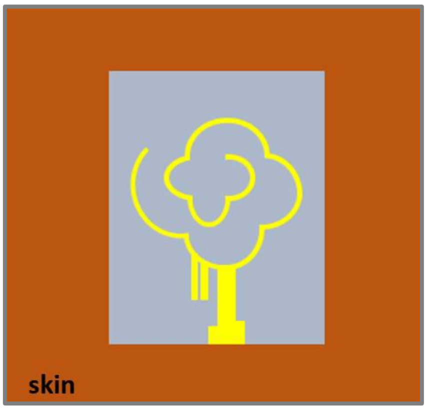

Fig. 9. The antenna on the skin layer.

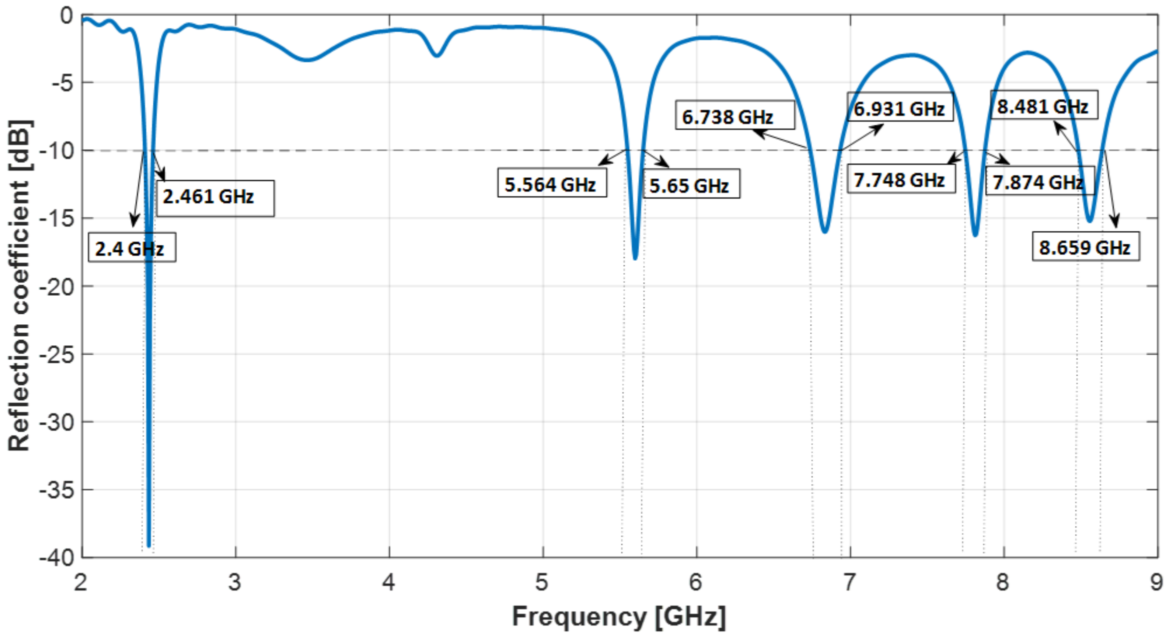

Fig. 10. The reflection coefficient S_{11} of the antenna on the skin layer.

3. PERFORMANCE AND ANALYSIS

In this section, the main evaluating parameters of the antenna performance are evaluated. In particular, the: gain, radiation efficiency and Specific Absorption Rate (SAR) are evaluated. A link budget is also calculated in this section with an indication of the maximum distance that the proposed antenna can support reliable communications over.

3.1. Radiation Characteristics

The total radiation efficiency and realized gain values at the center frequencies of the bands covered on the skin layer are: -14.48 dB and -8.88 dBi, respectively at 2.45 GHz, -7.39 dB and -1.24 dBi, respectively at 5.6 GHz, -5.25 dB and 1.32 dBi, respectively at 6.84 GHz, -8.63 dB and 0.38 dBi, respectively at 7.8 GHz, -7.187 dB and 1.21 dBi, respectively at 8.57 GHz. The far field radiation pattern at 2.45 GHz and the center frequency of all bands of operation is shown in Fig. 11.

The antenna achieves a radiation pattern directing out of the human body as desired at angles of 2 degrees at 2.45 GHz, 30 degrees at 5.6 GHz, 4 degrees at 6.84 GHz, 41 degrees at 7.8 GHz and 49 degrees at 8.57 GHz.

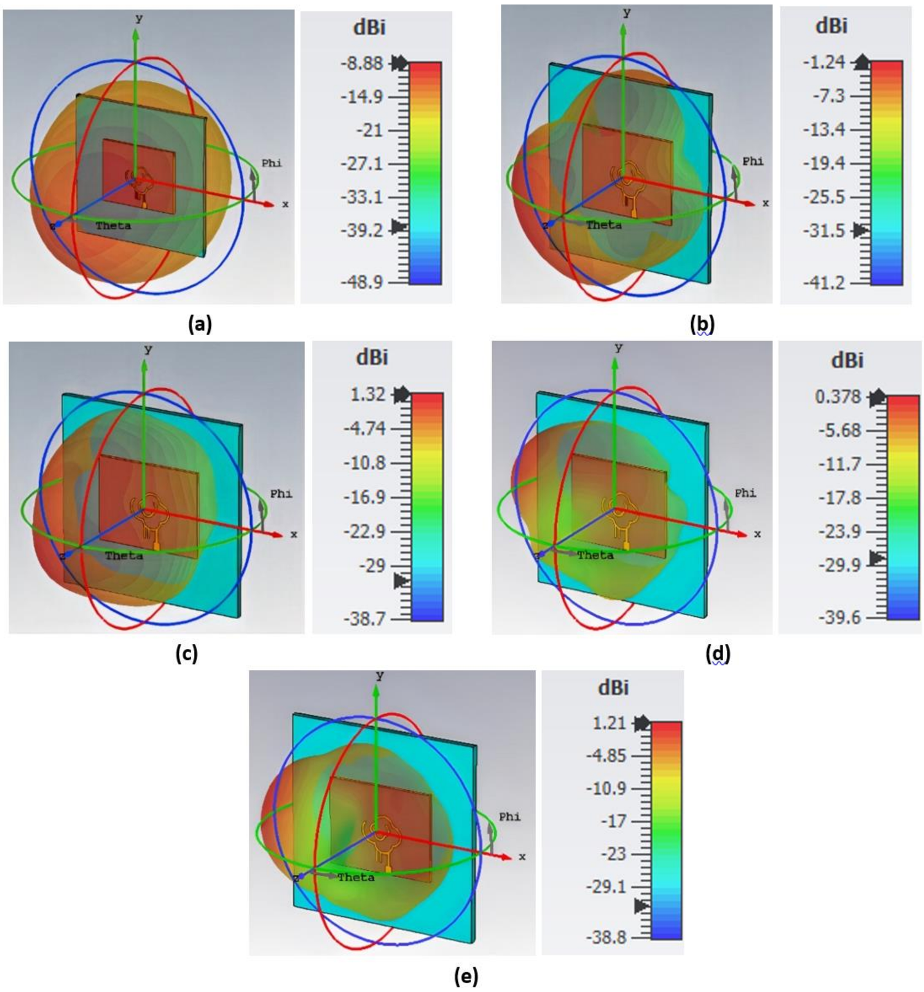

Fig. 11. The antenna gain pattern at: a) 2.45 GHz; b) 5.6 GHz; c) 6.84 GHz; d) 7.8 GHz; e) 8.57 GHz.

3.2. Validation in Multilayer Body Models

In this section, the performance of the proposed antenna is evaluated in two further body models:

- **The first body model:** is a multilayer body model composed of four layers which are: skin, fat, muscle, and bone. This body model is like that in [23]. The thickness and dielectric properties of each layer are provided in Table 2. Note that the dielectric properties of the human body tissues are frequency dependent and thus they are provided for each frequency [22]. The structure of this body model with the antenna on it is shown in Fig. 12.

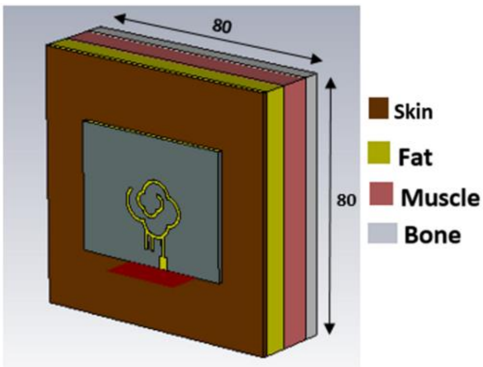

Fig. 12. The antenna on the multilayer (4-layer) body model (dimensions in mm)

Table 2. Dielectric properties of the first multilayer body model of validation.

Tissue layer	Thickness [mm]	Frequency [GHz]	Dielectric properties	
			Relative permittivity (ε_r), Conductivity, σ [S/m]	Mass density, ρ [kg/m^3]
Skin	1.6	2.4	ε_r = 38, σ = 1.46	1100
		5.6	ε_r = 35.3, σ = 3.55	
		6.84	ε_r = 34.2, σ = 4.7	
		7.8	ε_r = 33.4, σ = 5.6	
		8.57	ε_r = 32.6, σ = 6.4	
Fat	8	2.4	ε_r = 5.2, σ = 0.1	950
		5.6	ε_r = 5, σ = 0.28	
		6.84	ε_r = 4.9, σ = 0.36	
		7.8	ε_r = 4.8, σ = 0.43	
		8.57	ε_r = 4.7, σ = 0.48	
Muscle	10	2.4	ε_r = 52.7, σ = 1.74	1041
		5.6	ε_r= 48.75, σ = 4.7	
		6.84	ε_r= 47, σ = 6.3	
		7.8	ε_r= 45.8, σ = 7.5	
		8.57	ε_r= 45.8, σ = 7.5	
Bone	5.4	2.4	ε_r=11.4, σ = 0.4	1850
		5.6	ε_r= 9.8, σ = 1.1	
		6.84	ε_r = 9.2, σ = 1.4	
		7.8	ε_r= 8.9, σ = 1.6	
		8.57	ε_r=8.6 , σ = 1.8	

The results of the simulated reflection coefficient are shown in Fig. 13. The results indicate that a good matching has been still obtained. The deepest matching (S_{11}= -36.2 dB) is obtained at 2.441 GHz while a reflection coefficient of -18.3 dB is obtained at 2.45 GHz. A reflection coefficient of S_{11} < -10 dB has been obtained for all the other bands.

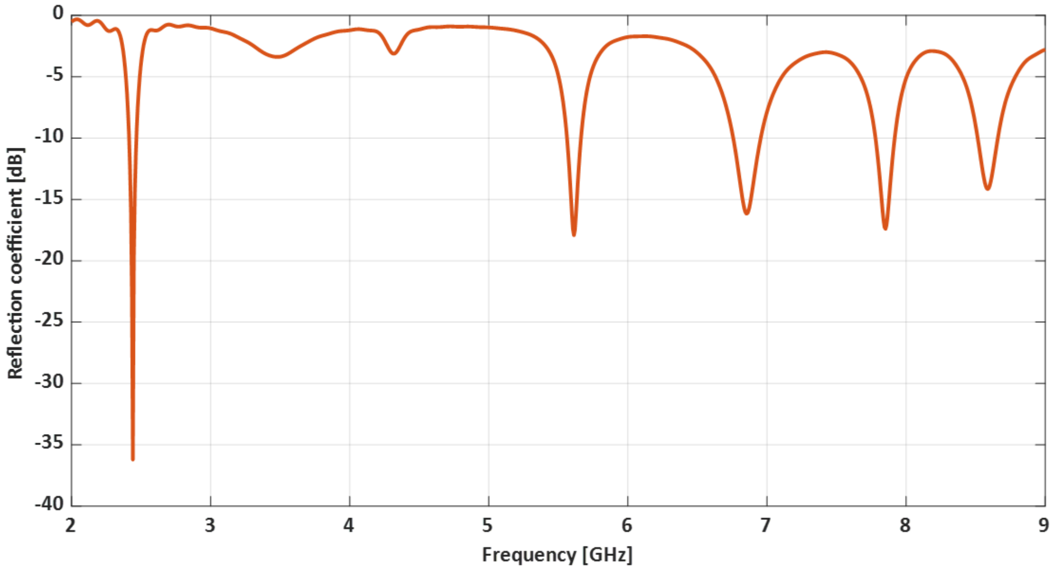

Fig. 13. The reflection coefficient S_{11} of the proposed antenna on the multilayer body model.

- **The second body model:** is a multilayer body model with a 6-layer human head model

To evaluate the antenna performance in proximity to the human head, a 6-layer human head has been modeled and the antenna is simulated inside of it. The model is shown in

Fig. 14. It is spherical in shape and is composed of 6 layers. It is like that in [24]. The thickness of each layer and its dielectric properties are summarized in Table 3 [24-25]

Table 3. The dielectric properties of the multilayer body model with a 6-layer head model.

Tissue layer	Thickness [mm]	Frequency [GHz]	Dielectric properties	
			Permittivity (εr), Conductivity, σ [S/m]	Mass density, ρ [kg/m^3]
Skin	1	2.4	ε_r= 38, σ = 1.46	1100
		5.6	ε_r= 35.3, σ = 3.55	
		6.84	ε_r = 34.2, σ = 4.7	
		7.8	ε_r= 33.4, σ = 5.6	
		8.57	ε_r= 32.6, σ = 6.4	
Fat	0.14	2.4	ε_r = 5.2, σ = 0.1	950
		5.6	ε_r= 5, σ = 0.28	
		6.84	ε_r= 4.9, σ = 0.36	
		7.8	ε_r= 4.8, σ = 0.43	
		8.57	ε_r = 4.7, σ = 0.48	
Bone	0.41	2.4	ε_r= 11.4, σ = 0.4	1850
		5.6	ε_r= 9.8, σ = 1.1	
		6.84	ε_r= 9.2, σ = 1.4	
		7.8	ε_r= 8.9, σ = 1.6	
		8.57	ε_r =8.6 , σ = 1.8	
Dura	0.5	2.4	ε_r = 42, σ = 1.67	1050
		5.6	ε_r = 38.1, σ = 4.1	
		6.84	ε_r= 36.6, σ = 5.3	
		7.8	ε_r= 35.5, σ = 6.3	
		8.57	ε_r= 34.6, σ = 7.1	
CSF	0.2	2.4	ε_r = 66.2, σ = 3.5	1060
		5.6	ε_r= 60.8, σ = 7.5	
		6.84	ε_r = 58.5, σ = 9.6	
		7.8	ε_r= 56.6, σ = 11.3	
		8.57	ε_r= 55.2 , σ = 12.7	
Brain	77.75	2.4	ε_r= 42.5, σ = 1.5	1030
		5.6	ε_r= 38.5, σ = 4	
		6.84	ε_r= 37, σ = 5.3	
		7.8	ε_r= 35.9, σ = 6.3	
		8.57	ε_r= 34.9 , σ = 7.2	

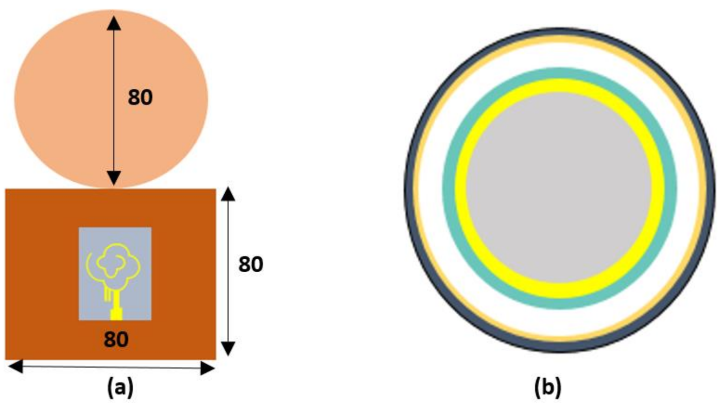

Fig. 14. The multilayer body model with a 6-layer human head model: a) Front view; b) cross section of the 6-layer head model (dimensions in mm).

The simulated reflection coefficient for this case is shown in Fig. 15. It can be seen from the figure that the matching levels have been slightly changed. However, they are still good enough to satisfy the -10 dB value of S_{11} for all the targeted bands.

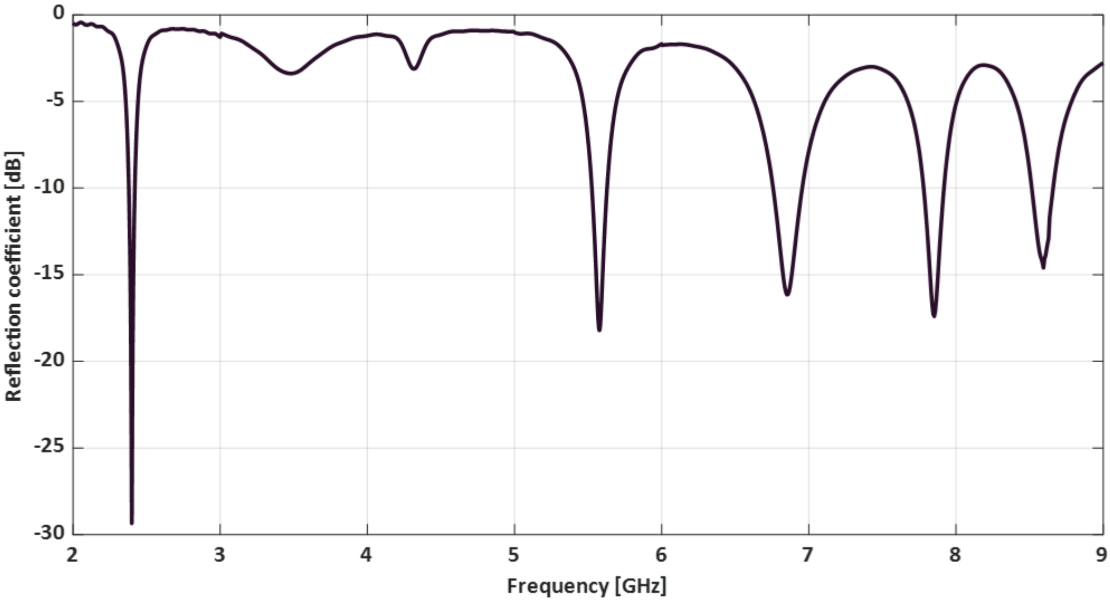

Fig. 15. The reflection coefficient S_{11} of the proposed antenna in the multilayer body model with the 6-layer human head model.

It is worth indicating that the antenna has obtained almost the same maximum 3D-gain and radiation efficiency at the center frequencies of all of the intended bands in the multilayer body model with and without the head. This is due to the ground effect that makes the antenna insensitive to the human body effect.

3.3. Specific Absorption Rate

As the antenna will be worn as a piece of a necklace on the human body, it is very important to evaluate the specific absorption rate (SAR). The SAR is calculated using [24]:

$$SAR = \frac{\sigma E^2}{\rho} \tag{7}$$

where σ [S/m] is the conductivity, E (V/m) is the magnitude of the near electric field and ρ (kg/m^3) is the mass density.

The maximum 1-g SAR is computed for the proposed antenna in the multilayer body model with the 6-layer head model. This is to evaluate the antenna effect on the human head and brain. The SAR distribution is shown in Fig. 16.

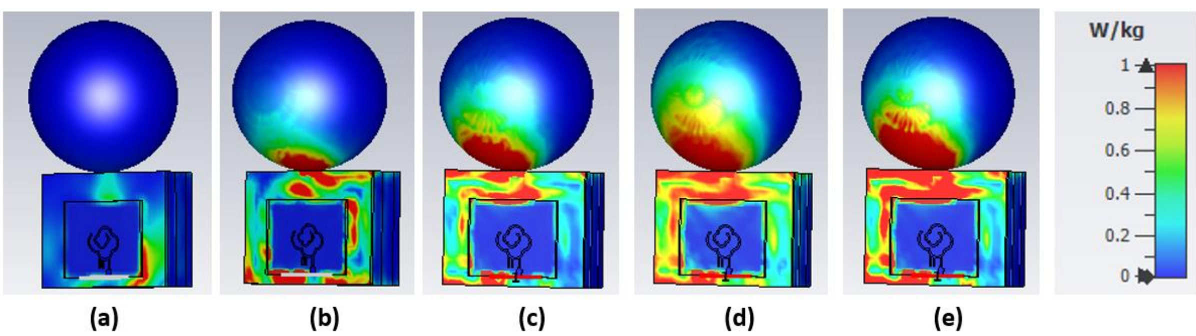

Fig. 16. The reflection coefficient S_{11} of the proposed antenna in the multilayer body model with the 6-layer human head model at: a) 2.45 GHz; b) 5.6 GHz; c) 6.84 GHz; d) 7.8 GHz; e) 8.57 GHz.

It can be seen from the figure that the SAR intensity in the human head increases with frequency. However, it is still concentrated in the outer shells of the head. In addition, these values are still small enough to support good levels of input power while satisfying the safety requirements. The maximum 1-g avg SAR values with the maximum input power that can be provided to the antenna is provided in Table 4.

Table 4. The simulated Max avg 1-g SAR in the multilayer body model with the 6-layer human head model.

Frequency [GHz]	Max 1-g avg SAR [W/kg]	Maximum allowed input power [W, dBm]
2.45	0.225	7.1, 38.5
5.6	1.03	1.55, 31.9
6.84	1.54	1.04, 30.2
7.8	2.06	0.78, 28.9
8.57	2.35	0.68, 28.3

It is worth indicating that the antenna was also designed over a smaller size of 30 mm by 40 mm. The smaller antenna obtained the same bandwidths and smaller gain and radiation efficiency of 1 dB only than that of the initial larger design.

3.4. Link Budget Calculations

The distance over which the proposed antenna communicate is calculated with reference to the following link budget equation [13]:

$$P_{rx} = P_{tx} + G_{tx} + G_{rx} - L_f - FM \tag{8}$$

where (P_{tx} (dBm)) is the input power to the antenna at the transmission end, G_{tx} (dBi) is the gain of the transmitting antenna, G_{rx} (dBi) is the gain of the receiving antenna, L_f (dB) is the free space loss and FM (dB) is the fade margin.

The free space loss (L_f) in dB is calculated as [13]:

$$L_f = 20\, log_{10}\left(\frac{4\pi df}{c}\right) \tag{9}$$

where f (Hz) is the operating frequency and c is the speed of electromagnetic waves in free space.

The link parameters and their values are provided in Table 5 [26].

Table 5. Link parameters for the budget calculations of the proposed antenna.

Link parameter	Symbol and Unit	Value				
Frequency	f [GHz]	2.45	5.6	6.84	7.8	8.57
Input power to the antenna	P_{tx} [dBm]	38.5	31.9	30.2	28.9	28.3
Gain of the transmitting antenna	G_{tx} [dBi]	-8.88	-1.24	1.32	0.378	1.21
Receiver sensitivity	P_{rx} [dBm]	-110				
Gain of the receiving antenna	G_{rx} [dBi]	2.13				
Fade Margin	FM [dB]	20				

Based on these values and their substitution in Eqs. (8) and (9), the distances over which the proposed antenna can communicate are calculated and provided in Table 6. It is obvious from the results in the table that the distance of communication decreases with frequency. This is because the free space loss increases with frequency. However, the results indicate that the proposed antenna can communicate effectively over a distance of longer than 3 km.

Table 6. The calculated distance of communication for the assumed link parameters.

Frequency [GHz]	Distance of communication [km]
2.45	11.92
5.6	5.878
6.84	5.313
7.8	3.599
8.57	3.365

3.5. Performance Validation Using Another Simulation Tool

The antenna performance is validated using another simulation tool which is Ansys High-Frequency Structure Simulator (HFSS). Ansys HFSS is a multipurpose, full-wave 3D electromagnetic (EM) simulation software [27]. Unlike CST which works based on Finite Integration Technique (FIT), HFSS works based on the Finite Element Method (FEM). However, results from both of HFSS and CST should match well for good and robust designs apart of the method used in each simulation software. Hence, simulations are also conducted using Ansys HFSS for the proposed antenna on the same multilayer body model in Fig. 12 under the same conditions. The results of the reflection coefficient are shown in Fig. 17. It can be seen from the figure that a deep reflection coefficient of equal to or less than -10 dB is obtained for all the intended bands. Also, it is worth indicating that almost the same gain values are obtained using both of HFSS and CST at the center frequencies of each band of interest.

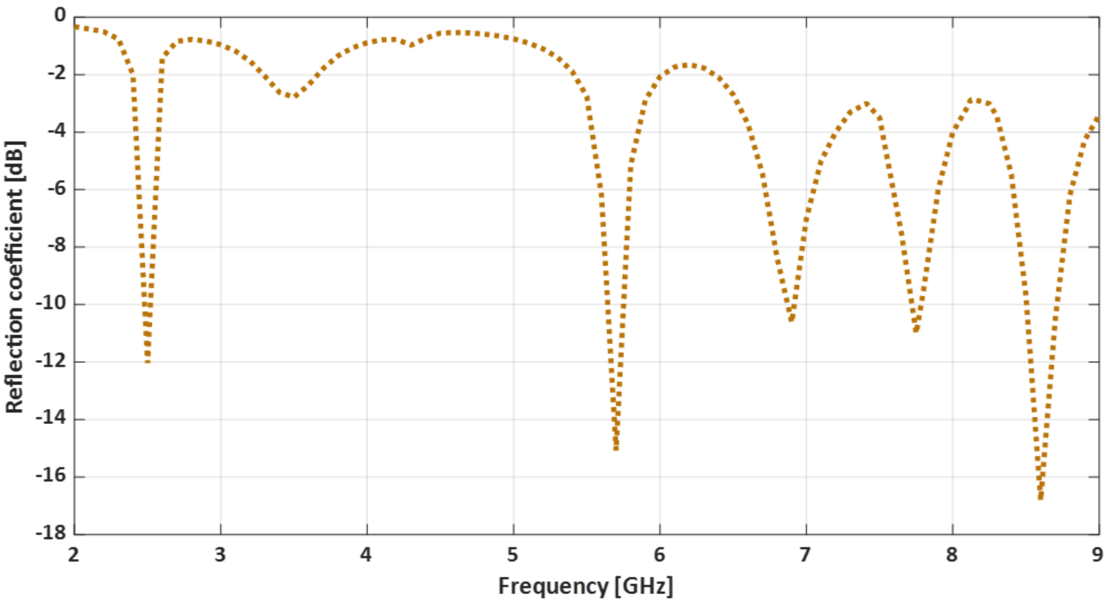

Fig. 17. The reflection coefficient S_{11} of the proposed antenna on the multilayer (4-layer) body model shown in Fig. 12 using Ansys HFSS.

3.6. Comparison with Previous Designs

The performance of the proposed antenna is compared with previous antennas proposed in literature. The comparison is summarized in Table 7. It can be seen from the comparison in the table that the proposed antenna can support a larger number of bandwidth than the other antennas of comparison. Although some antennas such as in [28] and [29] obtained larger gain, they were larger in size. The antennas in [30-33] obtained a larger gain over a smaller size, because they are exposed to a smaller lossy area of the human body (i.e. wrist). The antenna in [30] obtained a larger gain. However, that antenna was simulated on a body model of half the size of that of the proposed antenna in this paper. A few necklace antennas were proposed in literature. The antenna in [9] was small (10.5×7.5 mm^2) and of a relatively large gain (6.51 dBi). However, it worked at 29 GHz at which free space losses are large. Moreover, that antenna was not evaluated on the human body. A set of antennas were proposed in [10] as wearable necklaces. However, the presence of a head and chest model significantly reduced the radiation of the dipole antenna by 15 -30 dB. This is because the antenna had no ground which made it more susceptible to human body losses. The antenna in [34] had obtained a relatively good gain of 2.58 dBi. However, it was not evaluated on a human body model. To summarize up, the proposed antenna has many attractive features such as robust performance which is indicated by having: a good matching at the bands of interest and negligible variations in its radiation characteristics after evaluating it on the human body. This robust performance is attributed to the antenna ground that worked effectively to reduce the human body effect in correspondence with the results in [35]. The antenna has also the advantage of multi-band coverage. In addition, it supports communication over longer than 3 km.

Table 7. Comparison between the proposed and – the reported in literature - designs.

Ref.	Dimensions [mm]	Bandwidth [GHz]	Maximum 3D gain [dBi]	Type
[28]	43×85	2.4-2.5 4.75-6	1.7 -----	Logo tag conformal
[29]	40×210	0.4-0.46	4	Printed dipole
[30]	38×38	2.4-2.48	-2	Metal-cased smart jewellery conformal
[31]	28.81× 19.22 × 1.58	2.4-2.46 5.68-5.88	1 5.97	Smart watch strap Conformal
[32]	30×30×1.6	2.4–2.5 5.75–5.85	4.9 6.6	Smart watch patch Conformal
[33]	20×20×1.5	28-34	8.6	Multi-layer ring antenna Non-conformal
[34]	40×40×3.2	3.55-3.65	2.58	Snap-on buttons patch Conformal
[9]	10.5×7.5	27.9-30.99	6.51	Slot patch
[10]	153, 157	0.915	--------	Vee and Flex Dipole
This work	40×50	2.4-2.5 (5.564-5.65) (6.79-6.973) (7.7614-7.883) (8.5-8.65)	-8.88 -1.24 1.32 0.38 1.21	Flower-shape spiral conformal

4. CONCLUSIONS

In this paper, a spiral flower shape patch antenna is proposed for wearable IoT applications. The proposed antenna has the advantages of conformity, robust performance when placed on a simplified skin and multi-layer body models. It also supports multiple frequency bands in addition to the 2.45 GHz that is usually exploited for the intended application. The proposed antenna can be integrated to a wearable necklace which makes it conformal and easy to use for smart homes. The antenna has a number of appealing features such as robust performance and multi-band functionality which makes it a good candidate for wearable IoT applications. A relatively small level of specific absorption rate was obtained supporting a possible input power of 28 dBm.

REFERENCES

[1] R. Shrimali, "How IoT is Transforming the Healthcare Industry," *Telehealth & Healthcare IoT*, USA, 2020, https://embeddedcomputing.com/application/healthcare/telehealth-healthcare-iot/how-iot-is-transforming-the-healthcare-industry.

[2] N. Atanasov, G. Atanasova, B. Angelova, M. Paunov, M. Gurmanova, M. Kouzmanova, "Wearable antennas for sensor networks and IoT applications: Evaluation of SAR and biological Effects," *Sensors*, vol. 22, no. 14, pp. 1-19, 2022, doi: 10.3390/s22145139.

[3] *IEEE Standard for Safety Levels with Respect to Human Exposure to Radio Frequency Electromagnetic Fields, 3 kHz to 300 GHz*, 1999, https://ieeexplore.ieee.org/document/1626482.

[4] M. Ahmed, M. Ahmed, "A Wearable flexible antenna integrated on a smart watch for 5G applications," *Journal of Physics: Conference Series*, 2020, doi: 10.1088/1742-6596/1447/1/012005.

[5] M. Chung; C. Hsiao, C. Yang, B. Chuang, "4 × 4 MIMO antenna system for smart eyewear in Wi-Fi 5G and Wi-Fi 6e wireless communication applications." *Electronics*, vol. 10, no. 23, pp. 1-16, 2021, doi: 10.3390/electronics10232936.

[6] A. Semenov, O. Semenova, B. Pinaiev, R. Kulias, O. Shpylovyi, "Development of a flexible antenna-wristband for wearable wrist-worn infocommunication devices of the LTE standard" *Technology Audit and Production Reserves*, vol. 3, no. 1, pp. 20–26, 2022, doi: 10.15587/2706-5448.2022.261718.

[7] Z. Shuai, M. Sagor, "Wearable finger ring antenna array for 5G/mm wave applications, " IEEE International Conference on Telecommunications and Photonics, 2019, doi: 10.1109/ICTP48844.2019.9041740.

[8] Y. Seo, J. Cho, Y. Lee, J. Jang, H. Kwon, S. Kahng, "A chip antenna for Bluetooth earphones with cross-head interference tested from received-signal sensing," *Sensors*, vol. 22, no. 11, pp. 1-22, 2022, doi: 10.3390/s22113969.

[9] M. Rana, M. Rahman, "Design and Performance Analysis of a Necklace-Shape Slotted Microstrip Antenna for Future High-Band 5G Applications," International Mobile and Embedded Technology Conference, 2022, doi: 10.1109/MECON53876.2022.9752041.

[10] S. Nguyen, K. Yuk, R. Amirtharajah, G. Branner, "Radiation Patterns of an RF Energy Harvesting Necklace on Human Body Phantom," IEEE International Symposium on Antennas and Propagation & USNC/URSI National Radio Science Meeting, 2018, doi: 10.1109/APUSNCURSINRSM.2018.8608448.

[11] A. Serio, J. Buckley, J. Barton, R. Newberry, M. Rodencal, G. Dunlop, B. O'Flynn, "Potential of sub-GHz wireless for future IoT wearables and design of compact 915 MHz antenna," *Sensors*, vol. 18, no. 1, 2017, doi: 0.3390/s18010022.

[12] *CST-Computer Simulation Technology,* 2013, http://www.CST.com.

[13] A. Altarawneh, R. Alrawashdeh, "A Multilayer implantable patch antenna based on spiral split rings," International Workshop on Antenna Technology, 2022, doi: 10.1109/iWAT54881.2022.9811031.

[14] Y. Huang, K. Boyle, *Antennas from Theory to Practice*, Chichester: John Wiley & Sons Ltd, 2008.

[15] M. Sadiku, J. Buck, *Elements of electromagnetics*, London: Mcgraw hill higher education, 2012.

[16] W. Hayt, J. Kemmerly, S. Durbin, *Engineering Circuit Analysis*, New York: McGraw-Hill, 2012.

[17] H. Errifi, A. Baghdad, A. Badri, "Effect of change in feedpoint on the antenna performance in edge, probe and inset-feed microstrip patch antenna for 10 GHz." *International Journal of Emerging Trends in Engineering and Development*, vol. 1, no.4, pp. 80-93, 2014.

[18] A. Atser, J. Môm, L. Abiem, "Impact of feed point location on the bandwidth, frequency and return loss of rectangular microstrip patch antenna," *International Journal of Engineering Research and Technology*, vol.2, no. 9, pp. 1612-1616, 2013.

[19] A. Roy, P. Choudhary, S. Anand, P. Sarkar, S. Bhunia, "A novel approach on miniaturization of microstrip patch antenna with loaded strips," International Conference on Electronics, Communication and Instrumentation, 2014, doi: 10.1109/ICECI.2014.6767358.

[20] Y. Cao, Y. Cai, W. Cao, Z. Qian, L. Zhu, "Wideband microstrip patch antenna loaded with parasitic metal strips and coupling slots," *IEICE Electronics Express*, vol. 15, no. 15, pp.1-8, 2018, doi: 10.1587/elex.15.20180671.

[21] P. Prakash, G. Manoj, J. Samsonimmanuel, "MIMO Antenna System for IoT Applications (5G)," 6th International Conference on Devices, Circuits and Systems, Coimbatore, 2022, doi: 10.1109/ICDCS54290.2022.9780845.

[22] D. Andreuccetti, R. Fossi, C. Petrucci, "Calculation of the dielectric properties of body tissues in the frequency range 10 Hz - 100 GHz," *Institute for Applied Physics*, Italian National Research Council, Florence, Italy, 1997, http://niremf.ifac.cnr.it/tissprop.

[23] U. Pandey, P. Singh, R. Singh, N. Gupta, S. Arora, E. Nizeyimana, "Miniaturized ultrawideband microstrip antenna for IoT-Based wireless body area network applications", *Wireless Communications and Mobile Computing*, vol. 2023, pp. 1-19, 2023, doi: 10.1155/2023/3950769.

[24] A. Lak, H. Oraizi, "Evaluation of SAR Distribution in Six-Layer Human Head Model", *International Journal of Antennas and Propagation*, vol. 2013, pp. 1-8, 2013, doi: 10.1155/2013/580872.

[25] S. Anand, A, Ramprakash, K. Dhejonithan "Analysis of Specific Absorption Rate on Six Layer Human Head Model," *TechRxiv*, pp. 1-14, 2020, doi: 10.36227/techrxiv.12172833.v1.

[26] B. McAdams, "RF fundamentals for internet of things," *OleumTech*, 2017, https://www.microwavejournal.com/ext/resources/whitepapers/2017/May-17/OleumTech-White-Paper---RF-FUNDAMENTALS-for-IoT.pdf

[27] *Ansys HFSS- High-Frequency Structure Simulator*, 2019, https://www.ansys.com.

[28] G. Atanasova, B. Atanasov, N. Atanasov, "Fully textile dual-band logo antenna for IoT wearable devices," *Sensors*, vol. 22, no. 4516, pp. 1-19, 2022, doi: 10.3390/s22124516.

[29] A. Sabban, *Wideband wearable antennas for 5G, IoT, and medical applications*, in Advanced Radio Frequency Antennas for Modern Communication and Medical Systems. IntechOpen, 2020.

[30] T. Siddiqui, P. Khanal, L. Vähä-Savo, N. Lindvall, J. Holopainen, V. Viikari, "Bluetooth antenna for metal-cased smart jewellery," *Electronic Letters*, vol. 56, no. 3, pp. 115-117, 2020, doi: 10.1049/el.2019.2887.

[31] M. Shahzad, K. Paracha, S. Naseer,S. Ahmad, M. Malik, M. FarhanM, A. Ghaffar, M. Hussien, A. Sharif, "An artificial magnetic conductor-backed compact wearable antenna for smart watch IoT applications," *Electronics*, vol. 10, no. 23, 2021, doi: 10.3390/electronics10232908.

[32] B. Fady, A. Tribak, J. Terhzaz, F. Riouch, "Novel low-cost integrated multiband antenna design customized for smartwatch applications with SAR evaluation," *International Journal of Antennas and Propagation*, vol. 2020, pp. 1-14, 2020, doi: 10.1155/2020/8833839.

[33] F. Barneih, E. Majali, O. Alshaltone, N. Nasir, A. Al-Shammaa, "5G ring antenna for internet of medical things (IoMT) applications," International Conference on Developments in eSystems Engineering, 2021, doi: 10.1109/DeSE54285.2021.9719561.

[34] S. Chen, D. Ranasinghe, C. Fumeaux, "Snap-on buttons as detachable shorting vias for wearable textile antennas," International Conference on Electromagnetics in Advanced Applications (ICEAA), 2016, doi: 10.1109/ICEAA.2016.7731445.

[35] G. Casula, G. Montisci "A design rule to reduce the human body effect on wearable PIFA antennas" *Electronics,* vol. 8, no. 244, pp. 1-18. 2019, doi: 10.3390/electronics8020244.